Journal of Sea Research 204 (2025) 102563

Contents lists available at ScienceDirect

Journal of Sea Research

journal homepage: www.elsevier.com/locate/seares

Connectivity and larval drift across marine protected areas in the German bight, North Sea: Necessity of stepping stones

Vera Sidorenko [a,b,*], Sara Rubinetti [a,1], Anna Akimova [c], Bernadette Pogoda [d], Alexey Androsov [a,b], Kingsly C. Beng [c], Anne F. Sell [c], Santiago E.A. Pineda-Metz [d], K. Mathias Wegner [a], Sarah C. Brand [a], Lisa N.S. Shama [a], Jochen Wollschläger [e], Kerstin Klemm [f], Amin Rahdarian [g], Christian Winter [g], Thomas Badewien [e], Ivan Kuznetsov [b], Gerald Herrling [g,2], Silke Laakmann [f,e], Karen H. Wiltshire [a,3]

[a] Alfred Wegener Institute, Helmholtz Centre for Polar and Marine Research, Hafenstraße 43, 25992 List/Sylt, Germany
[b] Alfred Wegener Institute, Helmholtz Centre for Polar and Marine Research, Klußmannstraße, 27570 Bremerhaven, Germany
[c] Thünen Institute of Sea Fisheries, Herwigstraße 31, 27572 Bremerhaven, Germany
[d] Alfred Wegener Institute, Helmholtz Centre for Polar and Marine Research, Postfach 180, 27483 Helgoland, Germany
[e] Carl von Ossietzky University of Oldenburg, Ammerländer Heerstraße 114-118, 26129 Oldenburg, Germany
[f] Helmholtz Institute for Functional Marine Biodiversity, Ammerländer Heerstraße 231, 26129 Oldenburg, Germany
[g] Christian-Albrecht University of Kiel, Christian-Albrechts-Platz 4, 24118 Kiel, Germany

ARTICLE INFO

Keywords:
Lagrangian tracking
O. edulis restoration
Drifters
Tidal residual currents

ABSTRACT

This study investigated the transport of European flat oyster (*Ostrea edulis*) larvae between two Marine Protected Areas in the North Sea: Borkum Reef Ground (BRG), where oysters were recently reintroduced, and Sylt Outer Reef (SOR). Additionally, we determined the source of oyster genetic material collected during cruises in 2022 between BRG and SOR. To achieve these goals, numerical simulations focusing on surface and depth-averaged water mass transport were conducted using the FESOM-C coastal ocean model with a forward/backward Lagrangian module. Surface drifter data were also analysed to examine surface transport and validate the model output. Our results indicate that typical summer wind conditions, along with tidal residual currents, support the transport of water masses and passive tracers from BRG to SOR. Surface water masses from BRG generally approach SOR from the south and west. However, BRG and SOR are usually connected over periods exceeding two weeks, even considering the fastest surface currents. Strong and persistent south-westerly winds, which are uncommon in summer, can accelerate this connection to under two weeks. Conversely, strong and persistent easterly or south-easterly winds, also rare in summer, can prevent some passive tracers originating from BRG from ever reaching SOR or the eastern North Sea. In the case of depth-averaged transport, significantly more time is required, with a minimum duration of eleven weeks to connect the domains. This connection could be facilitated by an intermediary habitat - as a stepping stone in the transition zone, if that provides suitable habitat for settlement and subsequent larval production.

1. Introduction

The North Sea, in particular the German Bight, is a highly industrialized system supporting different services, namely: fisheries, transport and offshore energy, as well as regulating ecosystem services such as nutrient cycling, water and air purification, and climate regulation (Vogel et al., 2018; Wiltshire, 2017). During recent decades, tensions and conflicts have arisen due to competing interests, particularly in the allocation and utilisation of space for offshore wind farms, fishing and marine traffic, and the imperative need for conservation efforts to

* Corresponding author at: Alfred Wegener Institute, Helmholtz Centre for Polar and Marine Research, Hafenstraße 43, 25992 List/Sylt, Germany.
E-mail address: vera.sidorenko@awi.de (V. Sidorenko).
[1] *National Research Council of Italy—Institute of Atmospheric Sciences and Climate,* via *del Fosso del Cavaliere 100, 00133 Rome, Italy*
[2] *German Schleswig-Holstein State Agency for Coastal Protection, National Park, and Marine Conservation, Herzog-Adolf-Str. 1, 25,813 Husum, Germany*
[3] *Trinity College Dublin, Climate Sciences, Dublin 2, D02 PN40, Ireland*

https://doi.org/10.1016/j.seares.2025.102563
Received 17 August 2024; Received in revised form 5 January 2025; Accepted 6 January 2025
Available online 8 January 2025

protect ecosystem structure and biodiversity to ensure sustainable future development of the region (European Green Deal, 2024; EU blue economy report, 2023). The German Bight hosts several Marine Protected Areas (MPAs) with different protection status and governance, including the coastal Wadden Sea National Parks, the nature conservation area around Helgoland, and Natura2000 sites in the Borkum Reef Ground (BRG), Sylt Outer Reef (SOR) and Doggerbank in the German Exclusive Economic Zone of the North Sea (Krause et al., 2022).

Designated measures for the Natura2000 sites BRG and SOR include the restoration of the European flat oyster (*O. edulis*) and the reefs constructed by this bivalve (Pogoda et al., 2020; BfN: Bundesamt für Naturschutz, 2020a, b). SOR covers an area of 5.603 km^2 in the eastern German Bight consisting of coarse and medium sand areas, as well as reef structures at depths of 8–48 m (Hahn et al., 2022). BRG consists of sandy sediment interspersed with gravel, coarse sand, shingle beds and few reef-like structures over an area of 625 km^2 at depths of 18–33 m (BfN: Bundesamt für Naturschutz, 2020b; Fig. 1). Historically, oyster reef habitats covered extensive areas of the southwestern German Bight, extending from BRG to Helgoland and the Wadden Sea (Pogoda et al., 2020). Today, *O. edulis* is identified as functionally extinct in the German Bight, and targeted for restoration due to its role as one of the key species for the North Sea, supporting hotspots of biodiversity (e.g., Ref - OSPAR, 2020; Pogoda et al., 2019).

O. edulis is a mantle-brooding species, with larval release in the North Sea occurring over summer (from June to August) at temperatures between 15 and 20 °C (e.g. Maathuis et al., 2020; Colsoul et al., 2021). Each swarming event of *O. edulis* results in 0.1 to 1.8 × 10^6 larvae per female (Colsoul et al., 2021), each with a size of 160 to 200 μm, but reaching a size between 270 and 320 μm after a pelagic stage of 7–14 days, just before settlement (Colsoul et al., 2021). The duration of the pelagic phase is strongly temperature-dependent (De Mesel et al., 2018; Stechele et al., 2023) and determines the time a larva can potentially be transported to a new habitat before settlement (Beng et al. in prep.). Compared with temperature, the effect of salinity on larval growth is only minor (Robert et al., 1988). Experimental observations indicate that *O. edulis* larvae show systematic swimming behaviour that could affect their dispersal (Rodriguez-Perez et al., 2020). Finally, successful settlement depends on the availability of suitable habitat (Pogoda et al., 2023).

The recent interest in the restoration of *O. edulis* populations has resulted in significant research efforts dedicated to identifying suitable conditions and locations for restoration, as well as understanding the effects of restoration efforts on adjacent areas (e.g., Alter et al., 2023; Ermgassen et al, 2023; Hughes et al., 2023; Stechele et al., 2023; Pogoda et al., 2023). It is also known, that there is a connection between the considered MPAs based on the presence of other benthic organisms. Beermann et al. (2023) demonstrated that, for sandbanks, there are similarities between MPAs; however, there are also distinct community differences among them. However, while *O. edulis* larval release from restoration sites has been documented (e.g., Bos et al., 2023), no published evidence of settlement exists. In addition, larval transport by water currents from restoration sites, as well as hydrographic connectivity between MPAs, key aspects for restoration effort upscaling, lack quantification. One reason for this is the complex hydrodynamics of the German Bight, where nonlinear processes play a pronounced role. Tidal residual circulation or rectification currents despite general counter-clockwise direction along North Sea coast (e.g., Sprong et al., 2020; Visser, 1994), can be very complex, with many vortexes and locally reversed currents, so-called secondary currents. However, the atmosphere also significantly controls the transport and mixing processes in the German Bight. Westerly and south-westerly winds suppress the offshore spreading of surface coastal waters from the southern and eastern German Bight and forms an intense cyclonic (counter clockwise) wind driven circulation, which represents the dominant variability mode of the local circulation in the region (e.g., Schrum, 1997; Callies et al., 2017; Chegini et al., 2020). When north-easterly to south-easterly winds prevail, coastal water masses spread offshore. Moreover, the German Bight is directly influenced by the discharge of three relatively large rivers, the Elbe, Weser, and Ems, which contribute to temperature and salinity variability. Density gradients, both horizontally and vertically, also determines circulation patterns (e.g., frontal dynamics, tidal ellipses vertical structure) via baroclinic pressure gradients. There are periodic and non-periodic stratification events mediated by tidal and wind forcing (e.g., Schrum, 1997; Burchard and Hetland, 2010; Stanev et al., 2019; Chegini et al., 2020; Kopte et al., 2022), howevere, the areas with depths less than 20 m are generally well-mixed. When easterly and north-easterly winds dominate for several days, plumes from the Elbe and Weser can reach the island of Helgoland, resulting in a drop-in salinity and an increase in nutrients (e.g., Sidhu et al, 2023). Wind stress and stratification patterns can exhibit rapid fluctuations on short time scales (hours), necessitating the integration of specific time frames for predicting net transport.

Particle tracking models coupled with hydrodynamic models have been extensively used to study the transport of water masses and passive tracers (e.g., Fajardo-Urbina et al., 2023; Sprong et al., 2020), as well as pollutants like plastics (e.g., Bigdeli et al., 2022). They have also been used to investigate the dispersal of pelagic larvae across a range of marine organisms, including sessile species and fish (e.g., Bartsch et al., 1989; Akimova et al., 2019; Wang et al., 2022; Pastor Rollan et al., 2023). These models have proven especially valuable for studying connectivity between spawning and nursery grounds of marine fish and for examining the spread of non-indigenous species (e.g., Hufnagl et al., 2012; Schourup-Kristensen et al., 2023). Over the past few decades, such models have increasingly been used to assess the effects of human-made structures and marine protected areas on the dispersal, settlement, and survival of marine organisms during their early life stages (Fox et al., 2016; Molen et al., 2018; Mayorga-Adame et al., 2022). The accuracy of model-based assessments heavily relies on the ability of the utilized hydrodynamic models to capture fine-scale variability in the velocity field, as well as on existing knowledge of relevant biological traits of the studied species, such as their vertical positioning preferences and pelagic phase duration.

In the case of *O. edulis* larvae uncertainty in identifying the oyster larvae dispersal pattern arises from contradictory and incomplete information regarding larval preferences for their vertical position in the water column. While such information exists for other oyster species or specific developmental stages (e.g., Dekshenieks et al., 1996; Baker and Mann, 2003), it has not yet been integrated for the full duration of the larval phase of *O. edulis*. Furthermore, larvae can potentially change their depth preferences depending on their developmental stage, as well as the influence of abiotic factors such as temperature. In laboratory experiments, oyster larvae demonstrated the ability to control their buoyancy and to swim (up to a couple of cm/s) and may be present throughout the entire water column, albeit with a preference to remain near seabed (Rodriguez-Perez et al., 2020).

This study is aimed to:

1. Test the hypothesis that *O. edulis* larvae originating from the restoration site in the BRG could reach SOR within a single generation driven by ocean currents under typical wind conditions.
2. Determine the potential source regions of genetic traces of oysters collected during the spawning season (June–July) 2022 at BRG, SOR and between these MPAs.
3. Establish the physical connectivity between BRG and SOR MPAs in terms of surface and depth-averaged water mass transport and potential larval drift of *O. edulis*.

To achieve these goals, we analysed the drifters released in 2015, 2017–2021, and 2023 in the area of interest. Drifters are an important tool for investigating surface transport and studying surface circulation. We considered the drifters' paths as a proxy for larvae with preference to stay at the surface. Additionally, we used bulk zooplankton from nets

and pumps and environmental DNA (eDNA) filtered from sea water at different water depths to detect oyster larvae in BRG, SOR and transition areas in 2022 via metabarcoding and a mixture of species-specific real-time PCR (qPCR) and digital PCR (dPCR) approaches (details are given in Beng et al. in prep.). We further conducted a series of numerical simulations focusing on surface and depth-averaged transport since it is not clear whether larvae have preferences for a certain vertical position in the water column. The aims of the numerical experiments were (a) to reproduce the surface drifter trajectories, thereby validating model results; (b) to backtrack up to three weeks from locations where oyster material was identified under full forcing (tidal-, atmospheric-, baroclinic-) scenarios to define the possible initial source of larvae; and (c) to simulate the depth-averaged tidal residual circulation mediated and not mediated by the typical summer baroclinic pressure gradients as a background transport pattern persisting in the area. As a numerical instrument, we used the FESOM-C coastal ocean model (e.g., Androsov et al., 2019; Fofonova et al., 2019; Kuznetsov et al., 2020) equipped with a machine learning tool and a forward/backward Lagrangian module (Neder et al., 2022; Sprong et al., 2020). We also placed the results of the study into a broader context by relating the observed and simulated tracer trajectories to the typical summer wind forcing and baroclinic conditions.

2. Material and methods

This study is largely based on the field data from drifter experiments and simulated pathways. The term 'tracers' will be used for the simulated particles, while 'drifters' will refer to the observational data.

2.1. Drifter field experiments

This study used several drifter datasets from selected field campaigns, chosen based on the deployment of drifters in the areas of interest, i.e. BRG, SOR, and transition area between BRG and SOR (Fig. 1, 2 and 3) and formulated study goals. More specifically, drifter data were retrieved from the following campaigns:

1) 2015 campaign during the FS Heincke (AWI_Heincke, 2017) cruise HE 445: nine GPS tracking drifters were deployed in the German Bight at different times. Technical details about the drifters are provided by Callies et al. (2017) and data are freely available online in the PANGAEA repository (Carrasco and Horstmann, 2017). In this study, we considered 5 relevant drifters.
2) 2017–2021 campaigns: data were retrieved from the "Drifter_North_Sea_2017–2021" dataset freely available online on the PANGAEA repository (Meyerjürgens et al., 2023). Technical details about the drifters are provided by Meyerjürgens et al. (2019) while the database is discussed by Deyle et al. (2023).
3) 2023 campaign: two drifters were released on 28.06.2023 onboard R/V Senckenberg (SEN2319). In this study, we presented only one of them, as the other one closely follows the first in the domain of interest.

All considered surface drifters are equipped with underwater wings, allowing them to track the surface current within the upper 50 cm of the water column. The wind slip, which describes the influence of wind on drift, is 0.27 % of the wind speed (Meyerjürgens et al., 2019). So, the direct influence of winds on the drifters movement is minimal and generally negligible, except under conditions of very strong winds and breaking waves.

We considered drifters released during different seasons—not only early summer, when *O. edulis* larvae are present in the water column—because surface dynamics is largely driven by wind forcing, which can be similar across various seasons on a short-term scale (hours to days). Some chosen drifter pathways have been analysed in previous studies by Callies et al. (2017), Meyerjürgens et al., (2019, 2023), Stanev et al. (2019a), and Ricker et al. (2022). Here, we considered the drifters' paths primarily from the perspectives of our study goals. The drifters from 2015 and 2023 were used to reconstruct surface currents using a neural network and for validation purposes. All drifters are additionally used to analyse the hydrological connectivity between BRG and SOR via surface currents. Note that surface drifters are not directly influenced by vertical mixing like real passive tracers are. Also, they represent the surface Ekman dynamics (if winds from a certain direction persist for at least several hours, the direction of the drifter will be approximately 45° to the right of the wind direction due to the Coriolis pseudo-force), but not the full Ekman layer. However, for larval drift studies, the consideration of drifters can be advantageous, given a larvae's ability to control the buoyancy.

2.2. Observed wind data

The observed wind data used in this study were taken from the meteorological station of the German Weather Service (DWD) located on the island of Helgoland. Hourly measurements of wind speed and directions have been recorded since 1975 with an ultrasonic anemometer installed 10 m above sea level. The wind direction has a 10-degree resolution. Data from 2021 were discarded because of the large number of missing measurements.

2.3. Oyster occurrence identified by molecular tools

Water sampling from different depths for eDNA analysis and vertical zooplankton sampling using bongo nets (100 μm mesh size, 135 cm mouth opening) and pumps were conducted in the MPAs BRG and SOR and transit regions during June–July 2022 on the R/V Heincke (HE601), R/V Walther Herwig (WH457), and M/V Krebs Helios (Fig. 4). These samples were analysed using qPCR and metabarcoding techniques. As the starting points for back in time (backtrack) simulations, we used the locations where *O. edulis* larvae signals were identified via molecular analyses of only zooplankton samples (the vertical horizon of larvae material presence is not known). Such samples/locations, where *O. edulis* larvae signals were identified, are referred to as 'positive' here and below. In this work, we do not use positive eDNA samples for back in time simulations, as the oyster signal in these samples can come from any life stage. However, it is important to note that the positive eDNA samples were found only in BRG and close to BRG to the east at 2 locations (6.669715°E, 53.98042°N; 6.908103°E, 54.02491°N; Fig. 4) at the surface and near the bottom respectively.

In the current manuscript, we have utilized the available observations in a very limited sense—considering only the presence or absence of *O. edulis* larvae signals. The presentation of the sampling procedure of eDNA and zooplankton aboard, the description of the molecular analyses applied, and the detailed analysis of the samples will be addressed in Beng et al. (in prep.).

2.4. FESOM-C model

In this study, we used the coastal ocean model FESOM-C equipped with machine learning tool and a Lagrangian tracking module as a numerical instrument. FESOM-C is the coastal branch of the global Finite-volumE Sea-ice Ocean Model (Androsov et al., 2019; Kuznetsov et al., 2020; Fofonova et al., 2021). It solves 3D primitive equations in the Boussinesq, hydrostatic and traditional approximations for the momentum, continuity and density constituents based on mixed unstructured meshes.

2.4.1. Mesh and Bathymetry

The computational area spans from the Rhine region to the eastern border of the German Bight, reaching northward to Dogger Bank. The computational mesh was generated using the SMS software (SMS, 2024). The mesh contains approximately 487,000 nodes and comprises

approximately 61,000 triangles and 443,000 rectangles. The mesh horizontal resolution varies from 30 m around Helgoland and 50–100 m in the intertidal zone to a couple of kilometers near the open boundary in the deepest part of the domain out of the German Bight. The coastline was sourced from the European Environment Agency coastline dataset (EEA, 2024). Bathymetry was taken from European Marine Observation and Data Network (EMODnet, 2024) with data resolution of 150 × 150 m and 30 × 30 m for some subareas in the Wadden Sea.

2.4.2. Tidal forcing

Tidal forcing was taken from the TPXO 9 model (Egbert and Erofeeva, 2002; TPXO 9, 2024). The TPXO 9 atlas combines the 1/6° base global solution and the 1/30° resolution local solutions for all coastal areas, including our domain of interest and provides information about 15 harmonic constituents. All harmonics were included to generate elevation at the open boundary. The TPXO 9 tidal solution shows one of the best realizations for open boundaries for the North Sea (Fofonova et al., 2019).

2.4.3. Atmospheric forcing

The observational data on wind forcing at Helgoland is used in the Discussion to provide high-quality statistics for the central German Bight. Due to the larger area of interest for the simulations and analysis of drifters' behaviour, we used reanalysis data. Specifically, we utilized hourly wind stress and atmospheric mean sea level pressure from ERA5 (ERA 5, 2024). ERA5 is the fifth generation of atmospheric reanalysis produced by the European Centre for Medium-Range Weather Forecasts (ECMWF). It provides estimates of the global atmosphere on a regular grid of 0.25 degrees in latitude and longitude and has been recently updated to extend back to 1940. The data was provided by the Copernicus Climate Change Service, Climate Data Store.

2.4.4. Baroclinic pressure

Three-dimensional values of the potential temperature and salinity of the water for 2015 were retrieved from the Atlantic- European North West Shelf- Ocean Physics Reanalysis (0.111° × 0.067° spatial resolution) provided by the Copernicus Marine Service (CMEMSa: Atlantic-European North West Shelf-Ocean Physics Analysis and Forecast, 2024). For the 2022 and 2023, values were retrieved from the Atlantic - European North West Shelf - Ocean Physics Analysis and Forecast with 0.014° × 0.03° spatial resolution (CMEMSb: Atlantic-European North West Shelf-Ocean Physics Reanalysis, 2024). In both cases, June/July monthly averages were used. These data were further utilized to reconstruct the field of the average baroclinic pressure, the gradient of which is an important term to be considered in the momentum equation.

2.4.5. Surface currents reconstruction using neural network

The FESOM-C model simulates vertically-averaged horizontal velocities under the presence of wind and tidal forcing, and horizontal and vertical baroclinic pressure gradients at 20 vertical layers, which were then depth-averaged. Three-dimensional equations are considered only at the preliminary stage to initialize the baroclinic gradient (without time dependence). This gradient is integrated vertically and then applied in the vertically averaged dynamic equations. Subsequently, surface velocities were reconstructed using a fully-connected neural network. The recovery occurs based on a forward neural network with 3 hidden layers (e.g., Jain et al., 1996), featuring 20, 10, and 5 neurons. All hidden layers use a hyperbolic tangent sigmoid transfer function, while the output layer uses a linear activation function. The Levenberg–Marquardt algorithm is used as the learning function. The input features (8 in total) include the depth-averaged simulated velocities, logarithm of depth, sea level, wind stresses at 10 m above sea level, and mean wind stress within 4 h before the considered time moment. The summer drifters from 2015 and 2023 were used as a database for the training and validation. Sixty percent of arbitrarily chosen drifter velocities were used for training, while the rest were used for validation and test. The error curve exhibits an appropriate elbow shape (Fig. S3 in Supplementary Material). To calculate velocities from the drifter coordinates, the forward scheme was employed. Using the trained model, we calculated the surface currents for the domain of interest by providing the input fields at each numerical grid cell. The primary reason for using a neural network to reconstruct surface currents instead of simulating the full 3D case and using upper layer velocities lies in the consideration of the thin surface layer directly influenced by the atmosphere in the current study. For the FESOM-C model with σ vertical coordinates the thickness of the surface layer directly depends on the bathymetry. Representing the drifters' dynamics would require a complex interpolation procedure in this case.

2.4.6. Lagrangian tracking module

As a post-processing tool, a drift module (FESOM-C drift) was applied to estimate the trajectories of conservative particles in the Lagrangian representation using the FESOM-C results. The FESOM-C drift was developed recently and has already been successfully applied (Neder et al., 2022; Sprong et al., 2020). In this study, the modelled drift was based on snapshots of the calculated horizontal depth-averaged and surface velocities. The particle transport calculation was performed on the same computational grid as the computation of dynamic characteristics, without interpolation on a regular grid. In the first stage, all necessary information about the horizontal velocities was interpolated to the points with the coordinates of the particles. The new coordinates of the particles were determined after calculating the velocity vector acting on these particles backward−/forward- in time and then the process was repeated. No diffusion was introduced into the Lagrangian module for the current setup. The temporal resolution of the snapshots of velocity used to feed the Lagrangian model was ~0.12 h (465.625 s) for all experiments.

2.5. Model experiments

In this study, we performed four types of numerical experiments (Table 1, a to d). The experiments differ in the time-period covered, the applied forcing and the post-processing Lagrangian algorithm used to assess the transport. All details are summarized in Table 1 and below.

2.5.1. Performance visualization, forward tracking

Setup (a) was used to demonstrate the performance of the FESOM-C, neural network tool and Lagrangian module. With this set of experiments, we aimed to reproduce observed drifter trajectories from the end of spring to the summer of 2015. In 2015, the drifters were released in five different zones of the German Bight. One hundred tracer particles were released as clouds with a ~ 2.5 km radius at each of the five locations in the North Sea, at the same times and places where the drifters were released. The surface velocities reconstructed using the neural network are utilized by the Lagrangian module to simulate trajectories. The averaged trajectories for each cloud are shown in Fig. 1.

2.5.2. Tidal residual currents, forward tracking

Experiments (b) and (c) aimed to obtain tidal residual currents between BRG and SOR, both in the absence (b) and in the presence of density gradients (c). In the case of (c), the baroclinic pressure field was reconstructed based on the temperature and salinity fields from July 2022. In total, ~40,000 particles were released over the *entire* German Bight, at intervals of ~3.105 h during a complete lunar cycle spanning 29.5 days. The reasoning behind this is that the fate of a particle can strongly depend on the phase of the diurnal and lunar cycle (e.g., ebb, flood, daily inequality, spring or neap tide, etc.) at which the particle was released. Note, that the particles do not return to its original position after a flood-ebb cycle due to strong non-linearity in the system. A total of 228 realizations were conducted for both (b) and (c). Once all 228 experiments were completed, we calculated the vector from each particle's initial location to its final position after ~12.42 h (duration of

Table 1
Description of the Lagrangian tracking experiments.

Setup	Tracking type, task type	Forcing	Simulation duration of each experiment	Time slot	N of tracers for each experiment	N of Lagr. tracking experiments
(a)	*Forward, surface*	*Tidal, wind stress, atm. pressure, baroclinic pressure*	*15–65 days*	*May–July 2015*	*100*	*5*
(b)	*Forward, depth-averaged*	*Tidal*	*Tidal cycle (~12.42 h)*	*29.5 days (full moon cycle)*	*36,600*	*228*
(c)	*Forward, depth-averaged*	*Tidal, baroclinic pressure*	*Tidal cycle (~12.42 h)*	*29.5 days (full moon cycle)*	*36,600*	*228*
(d)	*Backward, depth-averaged, surface*	*Tidal, wind stress, atm. pressure, baroclinic pressure*	*21 days*	*June–July 2022*	*100*	*4*41*2*

the flood-ebb cycle). (Note, we used a time step of 465.625 s for velocity snapshots in each experiment to accurately resolve a ~ 12.42-h time frame.) This provided a residual Lagrangian transport vector field for each experiment, which can be referred to as tidal residual circulation when divided by the tidal period duration to yield a velocity dimension. These 228 fields often exhibited similar patterns due to the chosen time steps and intervals. For example, if particles were released at the beginning of a flood, their trajectories and final positions were quite consistent across most experiments with some variation of the magnitude of the displacement. The Lagrangian residual vector field from each experiment can be visualized as streamlines, assuming that after each tidal cycle, the particles move in a net sense but then begin a new cycle from the same tidal phase (the beginning of a flood in our example). The 228 experiments covered different scenarios many times; then the median was taken. The median was considered not for each location, but for the whole 228 vector fields.

2.5.3. Source locations of larvae, backtracking

In experiment (d), we conducted a 21-day backtracking simulation of passive tracers to explore the potential sources of the identified *O. edulis* larvae material considering both depth-averaged and surface scenario. For the depth-averaged Lagrangian simulations, we used raw velocity output from the FESOM-C model. For the surface Lagrangian simulations we utilized velocities reconstructed using neural network (see 2.4.5). The release dates matched the larval sampling dates (1st-3d of July 2022). Since the exact time of larval sampling was unavailable, we initiated particles every 15 min from 8 am to 6 pm (41 realizations) during the sampling day. For each realization and each of the four locations where larvae were identified, 100 tracer particles were released as a cloud with an approximate 5 km radius. Note that in BRG, there were several locations where larvae were identified, but they were mostly covered within this 5 km radius.

2.6. Validation

FESOM-C was tested and verified in numerous realistic experiments for the North Sea and idealised experiments, as reported in several studies (e.g., Androsov et al., 2019; Fofonova et al., 2019; Kuznetsov et al., 2020; Sprong et al., 2020; Fofonova et al., 2021). Particular attention was paid to the choice of the tidal forcing for the North Sea domain (e.g., Fofonova et al., 2019). For this work, we compared the simulated tidal dynamics with data from 46 tide gauges in the North Sea from EMODnet (EMODnet, 2024) by performing a Fast Fourier Transform (FFT) analysis. The median phase error across M2, S2, N2, O1, K1, Q1, M4, and MS4 semidiurnal, diurnal, and over-harmonics is 19°, and the median amplitude error is 0.011 m. It is noteworthy that the model captures the tidal dynamics in the coastal zones very well with an improvement over our previous study using a coarser mesh (Kuznetsov et al., 2020).

As mentioned before, 40 % of the drifters' data from 2015 and 2023 were used for validation. The root mean square error (RMSE) of the validation performance for the considered data is 0.03 m/s. Additionally, we visualized the results for 2015 by applying the Lagrangian tracking module. The simulated surface trajectories (Fig. 1, magenta curves) accurately replicate the direction of movement and dynamic specifics, such as the presence of loops and trajectory complications.

3. Results

3.1. Observed drifter trajectories and connectivity between BRG and SOR via surface currents

In this subsection, we considered surface drifters deployed at the BRG, SOR, and at the transitional areas in between, to analyse connectivity between the BRG and SOR via surface currents. Given that surface transport is largely determined by wind forcing, the analysis was done for drifters released in different seasons and the corresponding wind conditions were examined as well. Firstly, we considered the paths of drifters that were released in May 2015 in the transitional area between BRG and SOR, which also served for the validation of the simulated surface dynamics. Here, we provided a short description of their paths in relation to the connectivity question and wind forcing influence (an additional analysis of their trajectories can also be found in Callies et al. (2017)). Then, we focused on the available drifters released directly from BRG. Finally, we provided an analysis of the drifters released in the area around Helgoland (a transition zone between BRG and SOR), where multiple tracers were released at the same locations with a 5-min interval.

In the end of spring and at the beginning of summer 2015, the drifters were released from the north and northeast of BRG (Fig. 1a-c) and in the vicinity of Helgoland (see Fig. 1d-e). From the 19th to the 23rd of May, south-westerly winds dominated, then from the 23rd to the 27th of May, winds became predominantly from the west-northwest (Fig. 1g). This is clearly reflected in the drifter trajectory shown in Fig. 1d (Supplementary Material Animation 1.1). Due to the persistent north-westerly winds since the 23rd of May (Fig. 1g), the drifter began to move south-southeast from the southern tip of SOR (Fig. 1d).

During the last days of May and the first week of June, south-westerly winds prevailed (Fig. 1 g) and enhanced the rapid northward and eastward movement of the drifters released from the north and northeast of BRG (Fig. 1a-c; Supplementary Material Animations 1.2–1.4). Over the next three weeks, rapid and multiple changes in wind direction resulted in the complex drifters' trajectories, forming loops and rapidly changing directions, spreading in the central part of SOR (Fig. 1a-c). These drifters (Fig. 1a-c) remained within SOR for more than three weeks, then they travelled first toward central/north Denmark in the northeast, but ended up along the coast close to Sylt, Rømø, or Mandø Islands due to strong north-westerly winds blowing two days from the 9th of July (Fig. 1 g).

Drifter released relatively close to Helgoland (Fig. 1e) revealed a complex trajectory and eventually stopped along the coast in the southeast direction from the release site. Even though the drifter shown in Fig. 1b was released nearly at the same time as the drifter illustrated

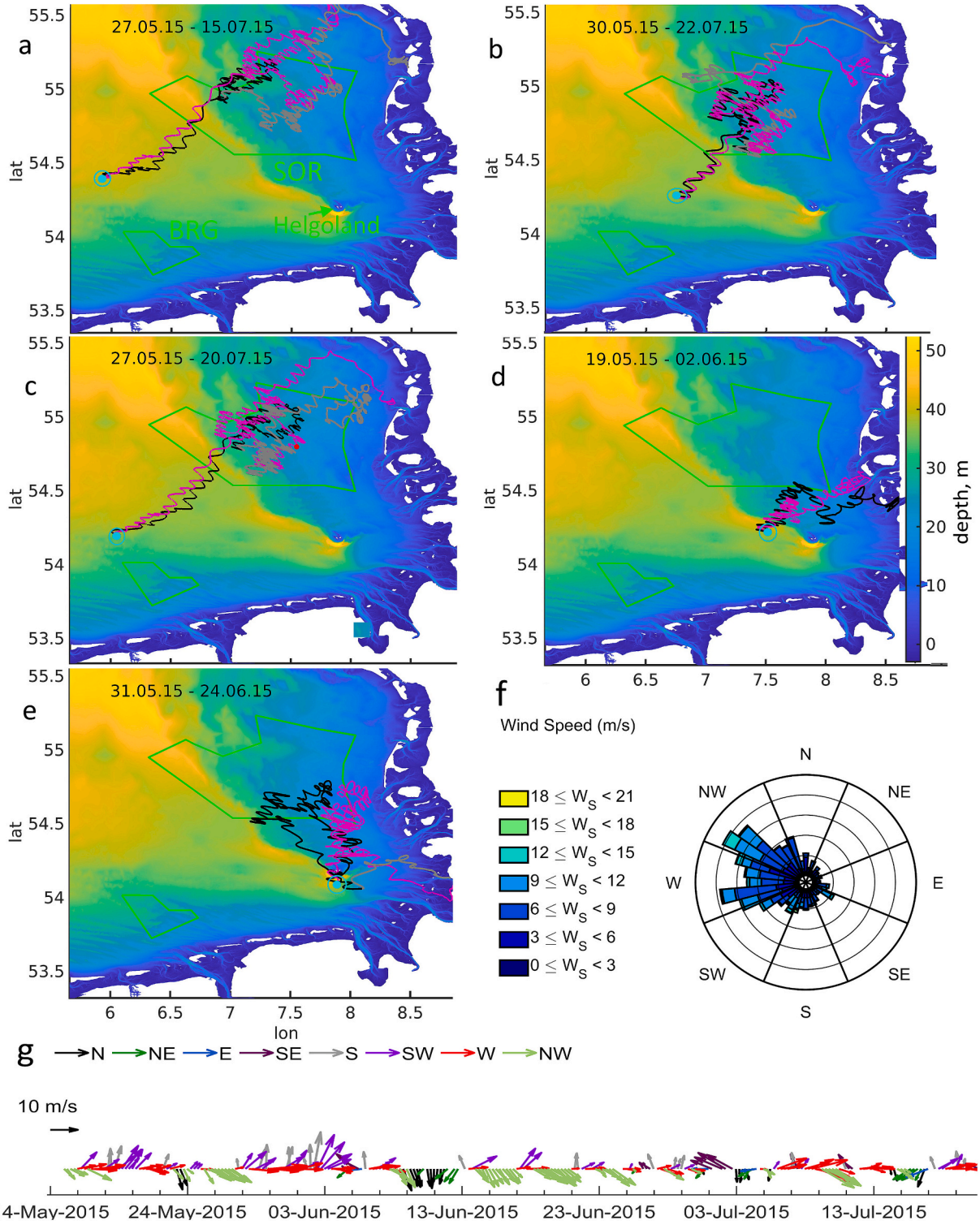

Fig. 1. (a-e) Observed (black-grey) and simulated (magenta) surface drifter/tracer trajectories in the German Bight superimposed on a bathymetry map [m]. Green lines show MPAs borders for BRG and SOR. The dates given on the top of each panel represent the time periods in which the drifters/tracers were considered. Cyan dots/circles indicate the release position of the drifters. Black colour indicates the trajectory within the first three weeks from the release. Grey colour indicates the fate of the drifters after 3 weeks. For the simulated course, the entire time period is coloured identically (magenta) for the sake of simplicity. (f) Wind rose of hourly winds data measured at Helgoland over the period 15.05.2015–15.07.2015. (g) Wind conditions during the drifters' travel. Arrows represent the 6 h average value of the wind. ('N' means northerly winds, 'NE' means north-easterly and etc.).

in Fig. 1e, their trajectories were noticeably different. The drifter released near Helgoland (Fig. 1e) first moved northward and then returned from the northwest to its original location after three weeks of travelling (see Supplementary Material Animation 1.5). It reflects that although the wind largely determines the drifters' paths, also other forces, such as tidal forcing or the presence of stratification, play a significant role.

Fig. 2 shows the fate of the drifters released from BRG during

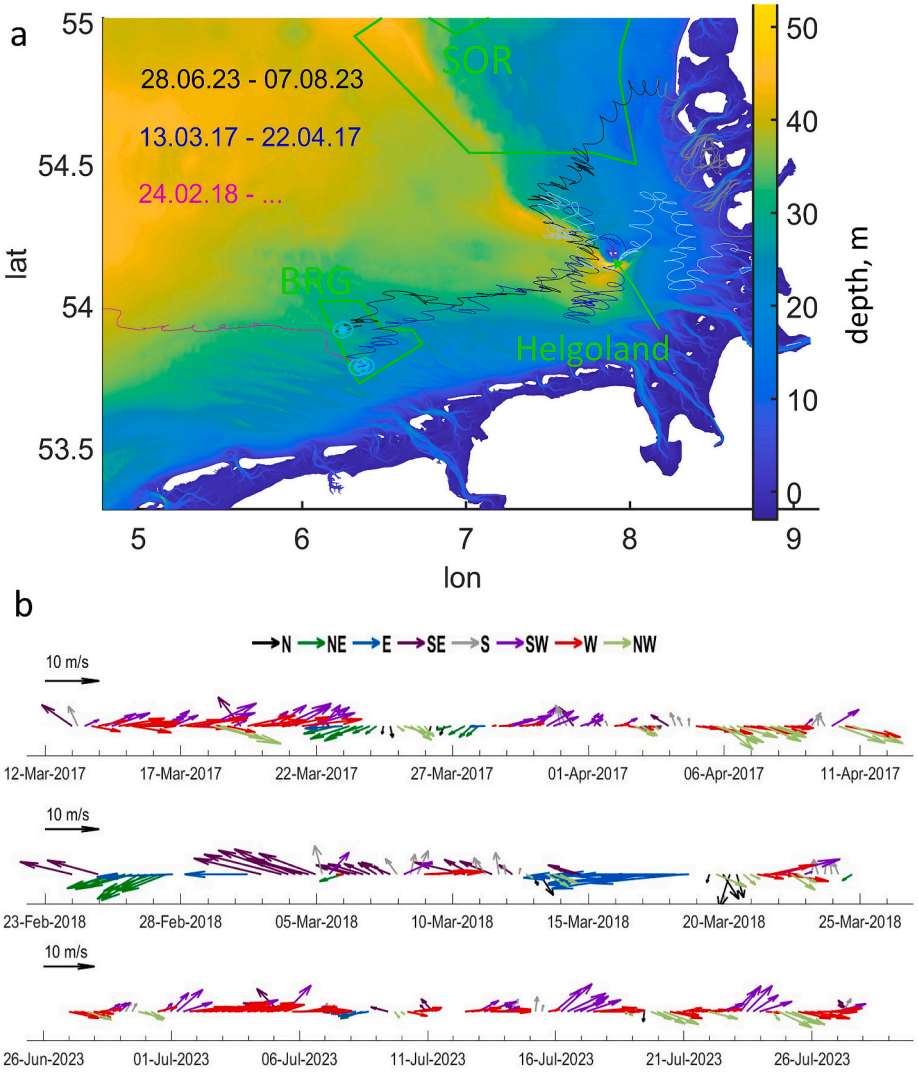

Fig. 2. (a) Drifter trajectories observed in 2017 (blue), 2018 (magenta) and 2023 (black) superimposed on bathymetry map, [m]. Cyan dots indicate the release positions of the drifters. Light blue and grey colours represent the trajectories of the drifters after three weeks from the release dates. Green lines show the borders of BRG (in the southwest) and SOR (in the northeast) MPAs. Note that the drifter from 2018 never returned to the area of interest; therefore, there is no end date provided here. (b) Wind conditions during the first 4 weeks of the drifters' travel. Arrows represent the 6 h average value of the wind. ('N' means northerly winds, 'NE' means north-easterly and etc.). (For interpretation of the references to colour in this figure legend, the reader is referred to the web version of this article.)

different years, compared here to explore the effects of different wind conditions. The drifter released in late June 2023 initially moved toward Helgoland, then toward the northwest, followed by a north-eastern path, and eventually southward. Drifter took approximately 3 weeks to reach the southern part of SOR from BRG (see Supplementary Material Animation 2). The drifter released in spring 2017 in the southern part of BRG nearly repeated the trajectory of the 2023 drifter until the area around Helgoland, where it made a loop in the south and then in the north from the island.

The prime reason of similarity between the trajectories is that in both cases westerly and south-westerly winds dominated during the first 10 days after the drifters' release (Fig. 2b). It is interesting to highlight the peculiar case of drifter released in February 2018 (Fig. 2a, magenta curve): it moved westwards contrarily to all the other cases reported here. The reason was extremely persistent easterly winds (Fig. 2b), which dominated over 3 weeks after drifter release. Note, that this drifter was travelling several months, but never came back to the area of interest.

Fig. 3 summarizes 26 trajectories of drifters released around Helgoland, an area that potentially can serve as a stepping stone for oyster larvae, during various seasons and years (2015, 2017–2019, 2021). Each subfigure (Fig. 3a-f) depicts the fate of drifters released at 5-min intervals and nearly at the same location. The cyan numbers indicate how many drifters were released at each location, suggesting repeated experiments with the same environmental forcing. Fig. 3a shows that the trajectories of two of the released drifters started to deviate from each other a couple of days after release (indicated by a red rectangle), yet the drifters met again at a later stage. Fig. 3c illustrates that eight released drifters initially moved together to the south (indicated by a red arrow); their trajectories then began to deviate, but all subsequently headed north, crossing SOR from south to northeast. Three of these ended up in the North Frisian Islands, while the others travelled further in a northwestern direction. Fig. 3b depicts the trajectories of drifters released on October 21st; these are similar to the drifters shown in Fig. 3a but were released 2 h earlier and south of Helgoland. Their paths largely mirror the behaviour of the drifters released 2 h later, although two of them ended up in the south-eastern Frisian Islands. Fig. 3e and f demonstrate cases where simultaneously released drifters nearly replicated each other's trajectories.

Considering Figs. 1, 2, and 3, we drew following important conclusions: (a) The drifters that approach Helgoland are highly likely to enter the SOR from the south-southeast and cross its eastern part. Among the

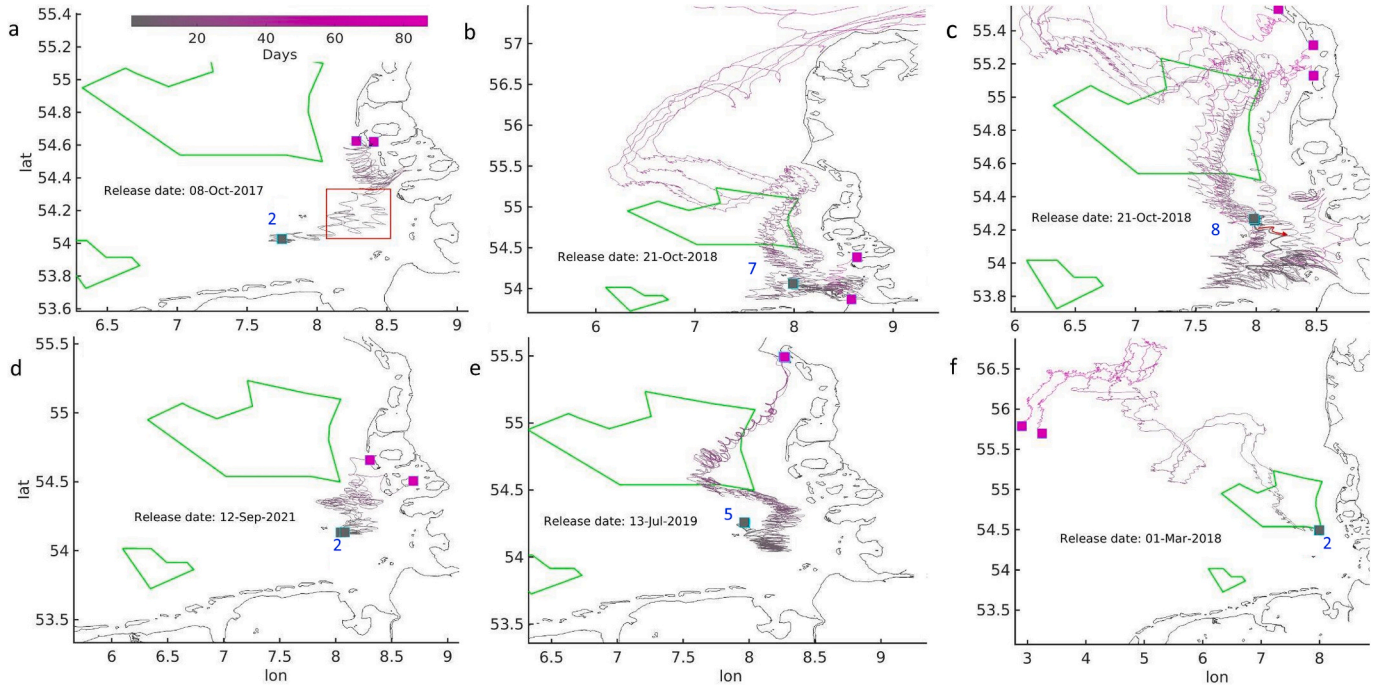

Fig. 3. The fate of the observed drifters released south of SOR, in the area around Helgoland, between 2017 and 2021. Grey boxes indicate the initial positions of the drifters; magenta boxes indicate their final position. Blue numbers indicate the number of the released drifters. Green lines show MPAs borders, in particular, borders of BRG (in the southwest) and SOR (in the northeast). (For interpretation of the references to colour in this figure legend, the reader is referred to the web version of this article.)

28 considered drifters being close to Helgoland, 21 reach the south-eastern SOR, with 18 of them crossing its eastern part. (b) The area around Helgoland represents a dynamically complex zone. Here, surface drifters are noticeably influenced not only by wind forcing but by other forcing players as well; the influence of tidal residual currents and baroclinic processes (e.g., the presence of frontal zones) is discussed in the next section. For instance, within different years and seasons, we observe a system of trajectory loops south of Helgoland (see Fig. 2a and Fig. 3b,c,e), and northward currents connecting the Helgoland area with SOR (Fig. 3b-e); additionally, we can notice spontaneous and significant deviations in the trajectories of closely following drifters (see Fig. 3a). (c) Drifters' trajectories begin to deviate significantly from each other in the shallow Wadden Sea (Fig. 3a-d), where nonlinear processes are stronger compared to the deeper areas. (d) The BRG is connected to the SOR via surface currents. Drifters released at BRG can approach the SOR from the south ('via Helgoland', as shown in Fig. 2 and 3) or from the southwest-west if they initially exhibit an east-northward movement (as depicted in Fig. 1). However, drifters released at BRG do not always reach the SOR or even the transition area in between, as illustrated in Fig. 2a (2018 drifter, magenta colour).

3.2. *Identification of potential source locations of larvae through backtracking analysis*

Fig. 4a displays the results of the backtracking simulations aimed at identifying the potential origin of oyster larvae sampled in summer 2022.

The backtracking analysis suggests that larvae sampled in the central-eastern part of SOR originated from the area to the south, considering surface currents. Similar to the surface drifters (see Fig. 3b, c,e), Fig. 4a demonstrates that the trajectories converge to the northwest of Helgoland. All backtracking trajectories consistently lead first to the southeast, toward Helgoland, and only afterwards the trajectories showed a larger spatial spread. In the case of tracers released in the western part of SOR, the backtracking cloud, considering surface currents, suggests that larval material have originated from the area between southwestern SOR and BRG.

The situation is significantly different when the depth-averaged currents are considered. In this case, the backtracking results show a very confined zone around areas where larvae signals were presented. Moreover, oyster larvae were predicted to come from the opposite direction compared to the surface backtracking when considering the western SOR (Fig. 4a, red curves). This is an expected outcome since the considered locations are relatively deep, especially in the western part of SOR, where the depth reaches 50 m. In a such deep area, surface currents are primarily driven by wind forcing, while the depth-averaged transport is predominantly determined by tidal forcing, this aspect will be further untwisted in the next sub-section. The depth-averaged solution largely assumes that the detected material, if originating from living larvae, came from SOR, that might indicate a presence of the spawning oysters in this area.

For BRG, the surface backtracking suggests larvae originated from either the Dutch side of BRG or from the Wadden Sea further south-southeast (Fig. 4a). Similar to SOR, the depth-averaged backtracking results suggest larvae originated close to where they were identified, potentially indicating self-attraction or self-sustainment.

In the transition zone, following the surface solution, larvae could have originated from the BRG or the Wadden Sea to the southeast, whereas the depth-averaged solution shows a confined and relatively narrow zone of origin.

In all four locations where oyster larvae were detected, the indicated origin of larvae, considering surface currents, was situated to the southwest from the sampling locations. This pattern is largely attributed to persistent westerly to south-westerly winds until middle of June and in the end of June/beginning of July (Fig. 4b).

Fig. 4a also shows the relatively large dispersion of the surface tracers in the Wadden Sea and south of Helgoland compared to the central part of the domain. This indicates that other forces, particularly tidal forcing, play a significant role in modifying transport patterns, especially in shallow areas and generally where non-linear terms are

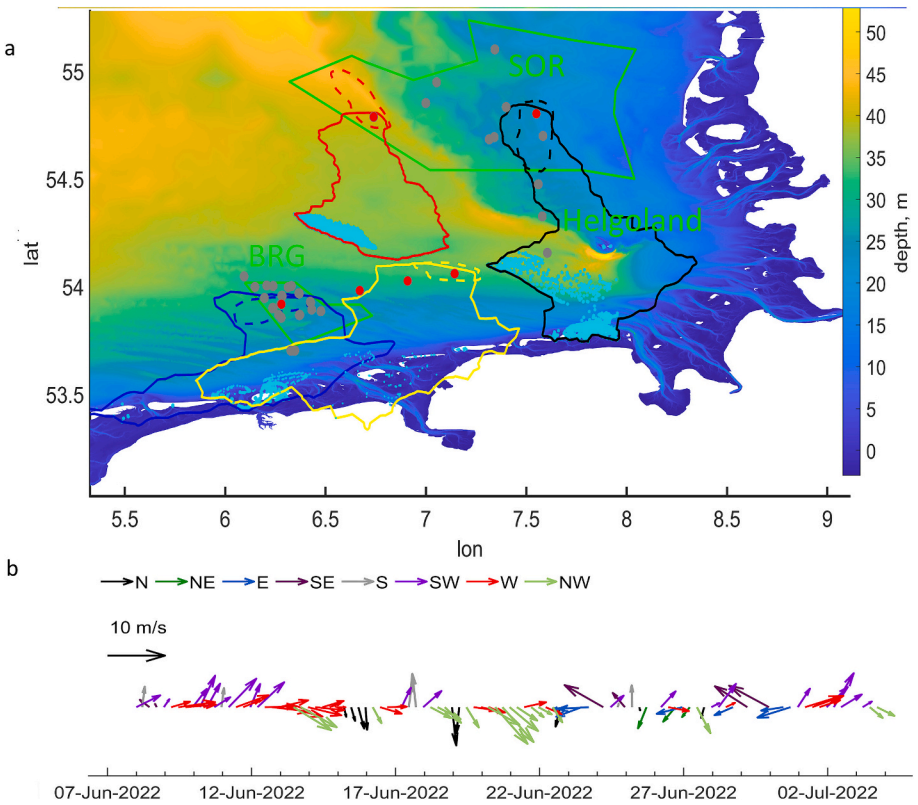

Fig. 4. (a) Clouds of the tracers, resulting from backtracking for 3 weeks in the summer of 2022 superimposed on a bathymetry map, [m]. Outlines in different colours indicate different locations of the backtracked tracer clouds. Dashed lines illustrate depth-averaged solutions, while solid lines illustrate solutions for the surface. Green lines represent the borders of the MPAs (BRG in the southwest and SOR in the northeast). Red dots identify positions where larvae were detected, for four locations the backtracking was performed. Grey dots mark the sampling positions where no larvae were detected. Turquoise dots show the positions of the modelled tracers 3 weeks before sampling. (b) Wind conditions during the period 01.07.22–21.07.22. Arrows represent the 6 h averaged wind speed and direction. ('N' means northerly winds, 'NE' means north-easterly and etc.). (For interpretation of the references to colour in this figure legend, the reader is referred to the web version of this article.)

strong, even when considering surface dynamics.

3.3. Tidal residual currents

Through the examination of observed drifters and simulated tracers, we found recurring transport patterns across different years and seasons, despite varying wind conditions. Additionally, we noted areas with extremely complex dynamics, where the interplay between the wind- and tide-induced dynamics, as well as baroclinic processes is fragile. In this subchapter, we aimed to clarify the role of the tide-induced net transport, which is expected to be significant in the German Bight given the large tidal amplitude, shallowness of the area, and complex topography. Furthermore, we considered the currents induced by baroclinic processes within the area of interest.

As mentioned in the introduction, stratification events in the middle of the German Bight occur due to the large discharge from the Elbe and Weser rivers and favourable south-easterly to north-easterly winds, which are more common in spring. Since we focused on the early summer season, we considered baroclinic processes only to a limited extent. Specifically, we examined depth-averaged tidal residual currents with and without baroclinic pressure gradients typical for the summer season.

Except for the zone around Helgoland, the Wadden Sea back barrier environment and estuaries, the trajectories induced by tidal forcing are elliptical (Supplementary Material Fig. S1). However, the tracers released at the specific location do not return to their original position after a flood-ebb tidal cycle. The direction in which the tracers move in a net or residual sense can vary depending on the timing of their release.

We calculated the median *net* transport induced by tides based on 228 experiments (Table 1) for both barotropic (Fig. 5a) and baroclinic (Fig. 5b) cases. This means that if tracers are released under tidal forcing at a specific location, they will generally move in a net sense as shown in Fig. 5; however, the trajectories can be complex (Supplementary Material Fig. S1). We conducted a barotropic depth-averaged experiment by releasing the tracers in the BRG and including only tidal forcing with another available model setup and grid, which confirmed our results (Supplementary Material, Convergence of the results; Supplementary Material Fig. S2).

Note that tidally induced velocities are much higher than shown in Fig. 5, in some areas of Wadden Sea they can reach 2 m/s. However, in this work we considered magnitude of residual circulation defined as the distance between the final and initial tracer locations, divided by the tidal period of 12.42 h.

The tidal forcing supports connectivity between BRG and SOR in both barotropic and baroclinic cases, particularly the connection from BRG to SOR, with an influx to SOR from the south and the west. However, the connection path is longer, via Helgoland, when typical summer baroclinic pressure gradients are taken into account.

Despite focusing on depth-averaged solutions in this subchapter, we observed that the obtained median tidal residual currents have a direct imprint on surface drifter trajectories (Fig. 1–3). Figs. 5a and b show a net-induced relatively strong transport of about 1–4 cm/s from Helgoland to the north, along with complex dynamics around Helgoland with a system of loops north and especially south of it in both baroclinic and barotropic cases, as can be also traced in Figs. 2 and 3 which reflect the behaviour of drifters. In both baroclinic and barotropic cases, there is a tidally induced net transport of about 5–10 cm/s from southern Sylt to the south. Notably, the drifter released in summer 2023 (Fig. 2a;

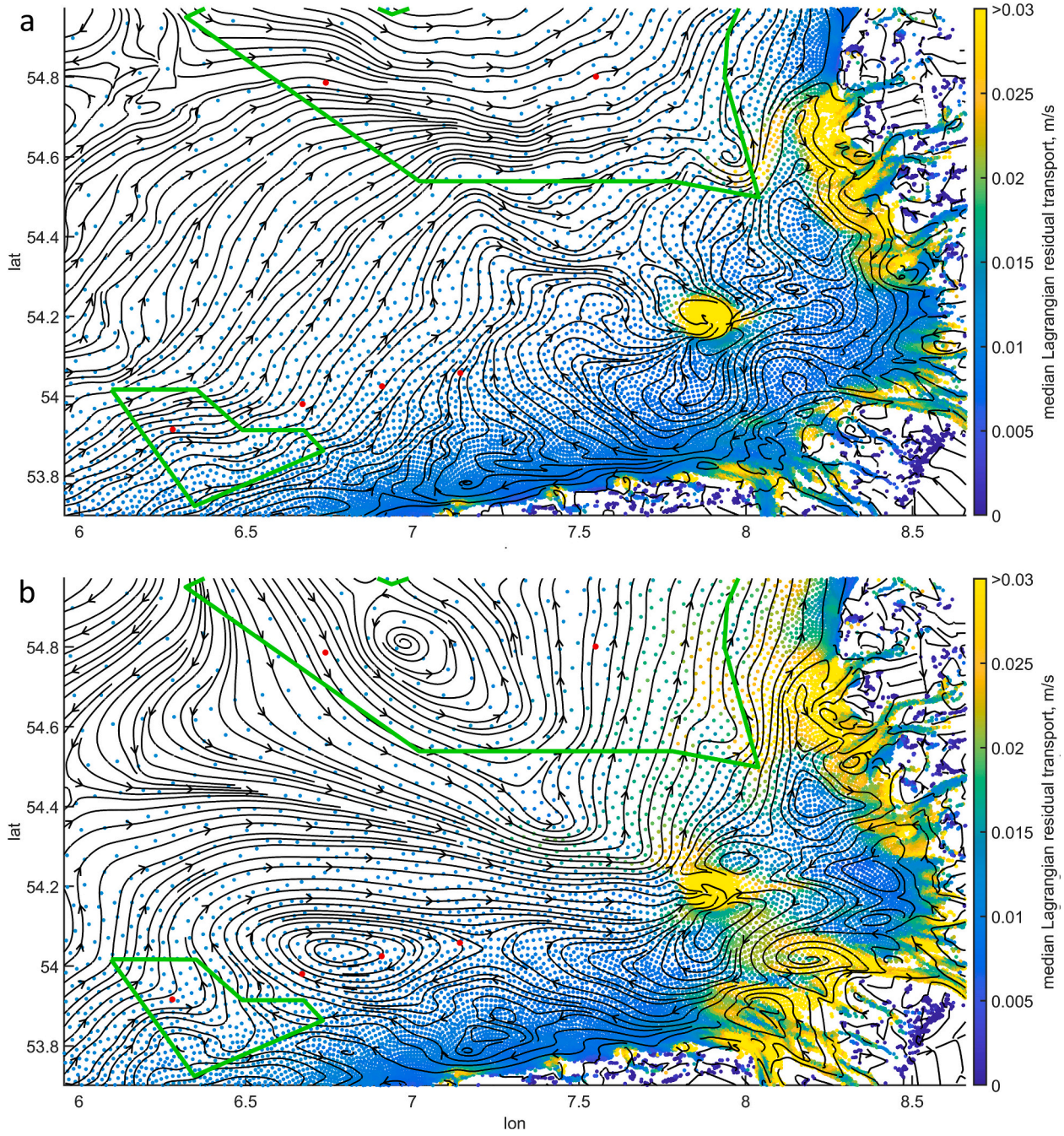

Fig. 5. The tidally induced median net transport, [m/s]: (a) barotropic case; (b) baroclinic case. The magnitude of the transport is calculated as the distance between the final tracer location and the initial location, divided by the tidal period (12.42 h). Green lines represent the borders of the MPAs. Red dots identify positions where larvae were detected. (For interpretation of the references to colour in this figure legend, the reader is referred to the web version of this article.)

Supplementary Material Animation 2) followed a trajectory similar to that identified in Fig. 5b, also depicting a tidally induced southward current along the North-Frisian Island. (Note, that there is also a buoyancy-driven current, mediated by the Earth's rotation, present in the area and flowing in the opposite direction. This current is relatively broad and not localised along the islands). The drifters' trajectories for the end of spring 2015 (Fig. 1 ac) align with the transport pattern identified in Fig. 5 as well. While the surface dynamics reveal the imprint of tidally induced transport, the depth-averaged backtracking solution (Fig. 4a) is largely determined by the pattern illustrated in Fig. 5b.

Even though the tidal residual currents (depth-averaged) in the area between BRG and SOR is generally not more than 2.5 cm/s, except in the Helgoland subarea where it reaches up to 20 cm/s, it's important to note that such a pattern tends to persist continuously over time.

4. Discussion

4.1. Physical connectivity

The tidal residual currents (Fig. 5) support the transport of water masses and *O. edulis* larvae from BRG to SOR; however, the connection time is longer than survival time of larvae. Additionally, our analysis of drifters and backtracking simulations (Figs. 1–4), which also account for wind forcing, suggests a high probability of connection from BRG to SOR via surface currents. Here, we need to discuss typical summer wind

conditions to generalize the results, the relationship between surface and depth-averaged transport, and provide additional quantifications.

4.1.1. Surface transport

In 2023, it took 2.5–3 weeks to connect BRG with the southern part of SOR via surface currents based on drifter data (Fig. 2). This is peculiar compared to the 50-year statistics of wind data. Specifically, as depicted in Fig. 6a, the percentage of total hours with winds blowing from the southwest—which are responsible for a fast water masses transport from BRG to SOR —is higher, while a lower percentage is associated with winds from the northwest compared to general statistics (Fig. 6b). A higher percentage of easterly winds was recorded in the days preceding the release of the drifters. The winds from northwest to east, which are missing during drifting time in 2023, can slow down to prevent respectively (Fig. 1, 2) the connectivity between the areas in the June–July period. Winds from the northwest are particularly common during the summer months (Fig. 6b; Rubinetti et al., 2023). These winds typically persist for 3–4 h in the same direction, on a median basis. However, considering the 95th percentile of the duration distribution, similar to the approach used in Rubinetti et al. (2023), during the summer season, winds from the northwest and north can persist for 27–34 h in the same direction. This suggests that in 2023, wind conditions were favourable for a relatively fast connection (~2.5–3 weeks) between BRG and SOR areas. Our additional experiments, focusing on 2 weeks periods in 2023 characterized by a strong dominance of southwesterly winds, demonstrated that it is possible to reach SOR within a two-week period considering surface currents (not shown). We should note that drifters always stay at the surface and do not experience vertical mixing, which a passive tracer in real ocean would undergo. Even though the drifters represent a good proxy for surface currents, they tend to overestimate the horizontal displacement of the passive tracer due to their insensitivity to wind-induced vertical mixing. Taking into account the mentioned considerations and *O. edulis* larvae's survival time of about two weeks, we do not support the hypothesis that the larvae originating in BRG could, under typical wind conditions, reach SOR within a single generation. In case of strong dominance of southwesterly winds, it can be potentially achieved. Backtracking simulations further support these findings. The potential location of the stepping stone could be around Helgoland (MarGate Underwater Observatory, 2024), south of Helgoland, or southwest of SOR, if the larvae are transported by surface currents.

The movement of surface tracers/drifters to the west (Fig. 2a, magenta curve), which suggests a complete absence of connection between BRG and SOR, is uncommon in summer. Corresponding winds from the northeast to southeast are less frequent compared to the winds from the west in the summer season (see Fig. 6b). Easterly winds typically persist for about 4 h, with extreme durations reaching up to 21 h (95th percentile of the duration distribution), whereas extreme persistence of the winds from southeast and northeast is much lower, ~10 h. Additionally, easterly winds should be strong and persistent enough—though the uniform thresholds for the entire area cannot be defined—to overcome the tidally induced transport. Nevertheless, in some years, easterly winds have been persistent. For instance, in 2008, winds blew from the east for about 20 % of the total time (while the typical percentage is 10 %, as shown in Fig. 6b). Similarly, in 1991, 1992, and 2019, winds were blowing from the east for about 17 % of the time. In terms of magnitude, winds from the west and northwest are associated with the highest speed values: ~7 m/s for the mean value and ~ 12 m/s at the 95th percentile of the probability distribution. Winds from the east also reach values of 11 m/s at the 95th percentile of the probability distribution.

4.1.2. Depth-averaged transport

In the depth-averaged case, much more time is needed to connect BRG and SOR (e.g., Fig. 4). It is also crucial to note that depth-averaged and surface back-tracking simulations yield significantly different results concerning the predicted sources of the observed larvae. This difference is attributed to the relatively deep areas under consideration, with depths reaching 50 m in SOR and 35 m in BRG. Without atmospheric forcing, it takes approximately half a year to connect the domain via the fastest route from northern BRG to southwestern SOR in a barotropic depth-averaged case. For a baroclinic case, this time is nearly doubled due to the longer route needed to connect the domains (Fig. 5a vs Fig. 5b). In both cases, the required time largely exceed the typical larval stage duration of *O. edulis*.

We considered two additional depth-averaged barotropic experiments with wind forcing characterized by the dominance of southwesterly and westerly winds, which are favourable for the fast connection between the domains. We simulated summer 1998 using the FESOM-C coastal ocean model, considering tidal and wind forcing. Additionally, we utilized existing setup for spring 2006 with tidal and wind forcing using the DELFT3D coastal ocean model (Supplementary

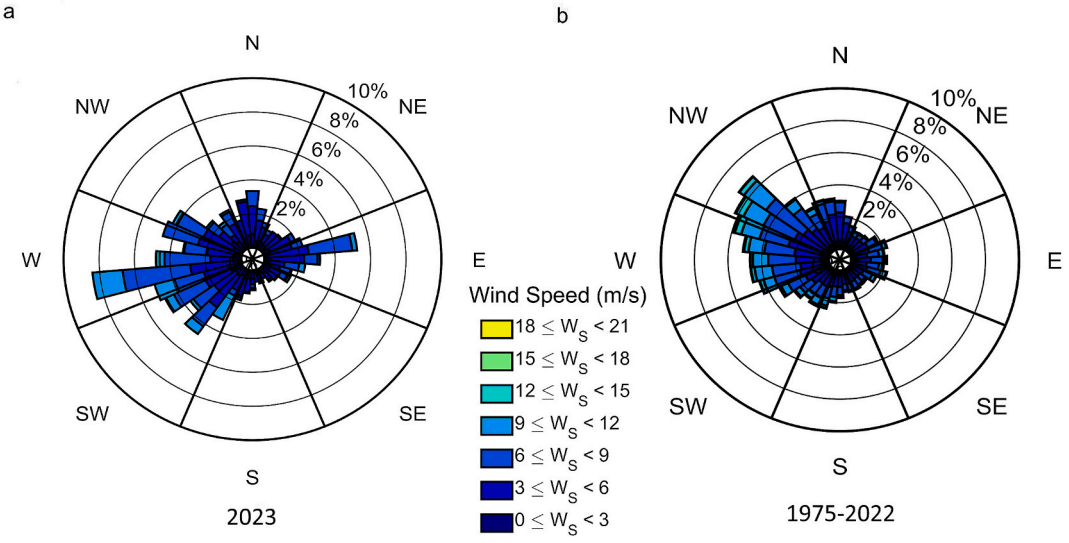

Fig. 6. Wind rose from hourly data measured at Helgoland during: (a) June–July 2023 period; (b) June–July months of the last 50 years (1975–2022).'%' indicates the frequency of occurrence of wind from a particular direction. (For interpretation of the references to colour in this figure legend, the reader is referred to the web version of this article.)

Material, Convergence of the results; Supplementary Material Fig. S2). Both summer 1998 and spring 2006 were characterized by a high percentage of duration of westerly to south-westerly winds that are favourable for the fast connection between two MPAs. In particular, during summer 1998 (June–July), the winds were south-westerly 27 % of the time and westerly to south-westerly 62 % of the time, with a 50-years median of 11 % and 35 % respectively (Fig. 6b). In spring 2006, the winds were south-westerly 24 % of the time and westerly to south-westerly 44 % of the time. On average, the drifting speed of tracers was modified by only ~2–6 % in these cases compared to the case with only tidal forcing. However, the net displacement of tracers from their original location increased by approximately two times when winds and atmospheric pressure were introduced due to stretching of the elliptical tidal-induced trajectories (Supplementary Material Fig. S1, S2). These numbers, of course, may vary with modifications in wind forcing. The travel time for the tracers to reach SOR from BRG, under current favourable wind conditions for fast connection between the domains, was about 11 weeks in both considered setups. Considering also that the barotropic case offers the fastest connection route (Fig. 5a vs Fig. 5b), we can conclude that 11 weeks is the minimum timeframe to connect the domains with a depth-averaged solution in the presence of favourable wind forcing. The depth-averaged solution suggests that larvae material identified at SOR and BRG are results of self-attraction or originating from non-living larvae.

It should be noted that if larvae drift to areas where the depth is about 20 m or less, depth-averaged and surface solutions become closer. In these shallow regions, tidal and wind forcing create a fully mixed water column. This means that the depth-averaged solutions identified for BRG and the transition zone in 2022 (Fig. 4, blue and yellow curves) can be significantly altered, potentially indicating a larger area of larval origin if the wind forcing varies, particularly in ways that push tracers toward shallower areas. In deeper areas in SOR, the near-bottom or middle water column position of larvae would imply higher retention within the area of origin with any forcing scenario. Therefore, understanding the vertical distribution of oyster larvae and its possible changes with larval ontogeny (e.g., surface or near-bottom) is essential to accurately simulate larval dispersal from the parental population. Additionally, we should note that while the depth-averaged solution serves as a useful proxy, it is not equivalent to the results obtained from full 3D simulations (e.g., Duran-Matute et al., 2024), which we plan to conduct in the future.

4.1.3. Depth-averaged and surface tidally induced transport

In this study, we simulated the median depth-averaged tidally induced transport. The tidally induced surface transport is much harder to define and is largely meaningless due to the strong and continuous impact of wind stress on the surface. In the absence of wind and vertical baroclinic structure, the vertically averaged velocities during almost the entire tidal cycle coincide in direction with the surface velocities. The three-dimensional velocity profile generally has a parabolic structure, tending to zero at the bottom and reaching a maximum at the surface, except during moments of significant change in tidal current direction. Because surface velocities are higher than the average velocities, their inertial component is somewhat higher. This leads to a substantial disruption of the parabolic profile at the moments close to the change in currents under tidal forcing. During these moments, lasting several tens of minutes, surface velocities can differ significantly from the average velocity in both direction and amplitude. This difference increases significantly in shallow areas because the turbulent layer there is more substantial relative to the full depth; in deep water, the vertical profile of horizontal velocities becomes closer to the average velocity. In the presence of atmospheric forcing and stratification, it is challenging to determine the coincidence of the direction and amplitude of the depth-averaged velocities and surface currents at all moments of the tidal cycle. However, we discuss above the instantaneous velocity profiles induced by tides, which do not generally provide information about transport. Transport is largely determined by the horizontal gradients of velocity components present within the tracer displacement during a tidal cycle. This means that all these facts only indicate that the surface tidally induced transport could be potentially different. On the other side, we see that depth averaged net transport induced by tides indeed is in agreement in a sense of direction with the drifters trajectories in the considered relatively deep areas of the German Bight (e.g., Fig. 1–3). The question about the magnitude of surface tidally induced transport remains unclear.

4.2. Abiotic conditions and O. edulis larvae dispersal

Abiotic conditions may influence the larvae's preference for their vertical position in the water column. While this question may be less significant in well-mixed conditions, where larvae cannot swim against currents vertically or horizontally, it becomes more pertinent in relatively deep zones where they may exhibit preferences for specific vertical positions. However, horizontal displacement would be still dictated by the ocean currents. Additionally, the time required for larval development depends on temperature, while the cumulative temperature experienced by adults prior to spawning seems to be most important for the timing of larval emergence (e.g., Robert et al., 2017; Maathuis et al., 2020; Alter et al., 2023).

In this study, we do not consider how other biotic and abiotic conditions, such as temperature, salinity, or food availability, influence larvae dispersal. These factors, along with the full range of summer forcing scenarios, including storm events, are the focuses of a separate studies. Additionally, the observations from 2022 were utilized only to identify the source of 'positive' samples and to partially explore the connectivity between the MPAs. A coupling of current hydrodynamic model with a biological model of oyster larvae and a full range of possible summer transport scenarios is a subject of an upcoming research (Beng et al. in prep.; Pineda-Metz et al., in prep.).

4.3. O. edulis larvae signal in the observations

It is worth noting that oyster larvae were observed at several stations in the German Bight, while they were often absent at neighbouring stations (Fig. 4). A similar observation was made in BRG, where known oyster beds exist (Fig. 4). Sampling larvae of marine organisms is technically challenging, so the absence data should be interpreted with caution. Also 'positive' signals require careful consideration, as observations may indicate the presence of larval material but not necessarily confirm the presence of living larvae. Further details on this topic are provided in Beng et al. (in prep.).

4.4. Historical background of oyster reefs in the German Bight

Our understanding of historical dynamics in marine environments remains limited. *O. edulis* is a benthic habitat- and reef-forming species, being once a key element of the North Sea ecosystem. Numerous historical sources give evidence of its former distribution and allow assumptions related to historical connectivity (Bennema et al., 2020; Lapègue et al., 2023). At the moment live oysters in the German Bight are confirmed at the BRG, Helgoland MarGate Underwater Observatory, and Danish coast.

The effect of obtained transport pathways can also be observed with other oyster species, such as the Pacific oyster, *Magallana gigas* (formerly *Crassostrea*). This non-native species colonized the North Sea in two separate, genetically distinct invasion waves (Möhler et al., 2011). One of these waves originated from Dutch aquaculture and spread along the southern North Sea toward east, while the other wave originated from the aquaculture activities on Sylt, from where it spread north- and southwards, colonizing large areas within a short period of time (Möhler et al., 2011; Reise et al., 2017).

This north-south split in dispersal routes reflects the directional split

in the tidally induced net transport (Fig. 5). It also demonstrates connectivity and outward exchange from the tidal inlet of the Sylt-Rømø to other areas of the North Sea. Historically, this area was rich in *O. edulis* beds. The current study strongly suggests that this area can be re-recolonized by the original oyster species in the future (Figs. 1–3, 5), although other factors such as environmental conditions, predation and competition should be taken into account.

4.5. Transport of larvae unrelated to ocean currents

Ships, mobile drilling rigs, and floating power farms have long been recognized as significant long-term homogenizers of coastal biota (Carlton, 1985; Baldwin, 1992). However, it is unlikely that they fulfil this role for *O. edulis*, based on published literature on settlement substrate preference (Colsoul et al., 2020; Ter Hofstede et al., 2024). Prior to settlement, larvae sink to settle in a hard substrate. As for the possibility of larvae being transported in the ballast water, this is also seemingly unlikely. *O. edulis* larvae, contrary to that of *M. gigas*, are more sensitive to pollutants, which reduces the chances of *O. edulis* larvae successfully developing in the ballast tank of ships. To address this question more comprehensively, careful long-term observations over a sufficiently large area, with statistical analysis of collected data, are required (e.g., Schourup-Kristensen et al., 2023).

5. Conclusions

Typical summer wind conditions (Fig. 6b) support the transport of surface water masses and passive tracers, such as *O. edulis* larvae, from BRG to SOR. However, BRG and SOR are usually connected over periods exceeding two weeks. During the summer season, surface water masses from BRG typically reach SOR from the south or southeast (Fig. 3, Fig. 5b). However, an intrusion of surface water masses originating from BRG to SOR can take place from the west and southwest in cases of prolonged south-westerly or southerly winds (Fig. 1a-c). Strong and persistent south-westerly winds, which are uncommon in summer, can accelerate the connection between considered MPAs to under two weeks. There is also a less frequent scenario where surface water masses originating from BRG do not reach SOR, particularly during periods when north-easterly to south-easterly winds prevail for an extended time (Fig. 2, magenta curve).

Tidal residual currents support transport from BRG to SOR and significantly determine it in a depth-averaged sense. However, the presence of typical summer horizontal and vertical density gradients makes this passage a bit longer via Helgoland compared to the barotropic scenario (where density gradients are not considered) (Fig. 5a vs Fig. 5b).

Our findings indicate that BRG and SOR can typically be connected over periods generally longer than the survival time of *O. edulis* larvae. It is especially relevant for the depth-averaged case: eleven weeks is the minimum timeframe to connect the domains in the presence of favourable wind forcing. Further investigation of potential habitat-connecting stepping stones like the area around Helgoland, as well as the current and future wind farms between BRG and SOR, is crucial and needs to be thoroughly considered. Based on our results, we anticipate that the wind farms located north of Helgoland, as well as those east and northeast of the BRG, could principally become future oyster beds, if the other components of habitat suitability are fulfilled. The aspect of hard substrates being introduced during the excessive construction of windfarms in the near future deserves particular attention with respect to their potential function as stepping stones for sessile benthic organisms with a planktonic egg or larval stage. In addition, the effects of species-specific biological and behavioural constraints need to be addressed.

The dispersion of drifters at the surface and tracers, both in the depth-averaged and surface solutions within particular period of time, is generally largest in the shallower zones of the German Bight, back-barrier Wadden Sea environment, and generally in areas where nonlinear hydrodynamic processes play a large role (Fig. 3, Fig. 4a, Fig. 5).

In all four locations where oyster larvae were detected based on zooplankton samples, the source of the larval material, considering surface currents, lies south-west of the sampling locations. This pattern is largely attributed to persistent westerly to south-westerly winds in the beginning of June and in the end of June/beginning of July 2022 (Fig. 4b). The depth-averaged backtracking results suggest larvae originate close to where they were identified, indicating a potential for self-attraction or self-sustainment (Fig. 4a).

CRediT authorship contribution statement

Vera Sidorenko: Writing – original draft, Visualization, Methodology, Investigation, Formal analysis, Conceptualization. **Sara Rubinetti:** Writing – review & editing, Visualization, Methodology, Formal analysis. **Anna Akimova:** Writing – review & editing, Formal analysis, Conceptualization. **Bernadette Pogoda:** Writing – review & editing, Investigation. **Alexey Androsov:** Writing – review & editing, Methodology. **Kingsly C. Beng:** Writing – review & editing, Data curation. **Anne F. Sell:** Writing – review & editing, Conceptualization. **Santiago E.A. Pineda-Metz:** Writing – review & editing, Data curation. **K. Mathias Wegner:** Writing – review & editing, Resources, Data curation. **Sarah C. Brand:** Writing – review & editing, Data curation. **Lisa N.S. Shama:** Writing – review & editing, Resources, Data curation. **Jochen Wollschläger:** Resources, Data curation. **Kerstin Klemm:** Resources, Data curation. **Amin Rahdarian:** Writing – review & editing, Visualization, Methodology. **Christian Winter:** Writing – review & editing, Methodology. **Thomas Badewien:** Resources, Data curation. **Ivan Kuznetsov:** Methodology. **Gerald Herrling:** Methodology. **Silke Laakmann:** Writing – review & editing, Resources, Investigation. **Karen H. Wiltshire:** Writing – review & editing, Supervision, Resources.

Declaration of competing interest

The authors declare that they have no known competing financial interests or personal relationships that could have appeared to influence the work reported in this paper.

Acknowledgements

All authors acknowledge support by the Federal Ministry of Education and Research (BMBF), Germany, through the project CREATE (03F0910A, 03F0910B, 03F0910C and 03F0910M) part of the research mission 'Protection and Sustainable use of Marine Areas' within the German Marine Research Alliance (DAM). K.H.Wiltshire, V. Siderenko, and A. Akimova also acknowledge support by the BMBF through the CoastalFutures project (03F0911J, 03F0911D). The work is also supported by the MGF-Nordsee (03F0847A) project in frame of DAM mission.We thank the captain and the crew of R/V Heincke (HE601), R/V Walther Herwig (WH457), R/V Senckenberg (SEN2319) and R/V Krebs Helios. The authors are grateful for the teams operated the AWI Marine Stations Helgoland and Sylt (Dummermuth et al., 2023).

Appendix A. Supplementary data

Supplementary data to this article can be found online at https://doi.org/10.1016/j.seares.2025.102563.

Data availability

The DWD data can be downloaded from. https://opendata.dwd.de/climate_environment/CDC/observations_germany/climate/. The Helgoland stations are 02100 and 02115. The drifter data, except drifter data from 2023, can be found in the PANGAEA database: https://doi.pangaea.de/10.1594/PANGAEA.874511, https://doi.pangaea.de/

10.1594/PANGAEA.963166 (Carrasco and Horstmann, 2017; Meyerjürgens et al., 2023). The drifters data for 2023 will be also available at the PANGAEA in 2024, at the moment are available under request. The version of FESOM-C v.2 used to carry out simulations reported here can be accessed from ZENODO data portal (Androsov et al., 2018). References to forcing, open boundary conditions, coastline, and bathymetry data are available throughout the text. The direct links are provided in the References section.

References

Akimova, A., Hufnagl, M., Peck, M., 2019. Spatiotemporal dynamics of predators and survival of marine fish early life stages: Atlantic cod (*Gadus morhua*) in the North Sea. Prog. Oceanogr. 176, 102121. https://doi.org/10.1016/j.pocean.2019.102121.

Alter, K., Philippart, C.J., Teng, S., Bolier, H., Drenth, P., Dubbeldam, M., 2023. Consequences of thermal history for growth, development and survival during metamorphosis and settlement for the European flat oyster. Aquaculture 566, 739174. https://doi.org/10.1016/j.aquaculture.2022.739174.

Androsov, A., Fofonova, V., Kuznetsov, I., Danilov, S., Rakowsky, N., Harig, S., Brix, H., Wiltshire, K.H., 2018. FESOM-C (Version v2). Zenodo. https://doi.org/10.5281/zenodo.2085177.

Androsov, A., Fofonova, V., Kuznetsov, I., Danilov, S., Rakowsky, N., Harig, S., Brix, H., Wiltshire, K.H., 2019. FESOM-C v.2: coastal dynamics on hybrid unstructured meshes. Geosci. Model Dev. 12, 1009–1028. https://doi.org/10.5194/gmd-12-1009-2019.

AWI_Heincke: Alfred-Wegener-Institute Helmholtz-Zentrum für Polar- und Meeresforschung (AWI), 2017. Research vessel HEINCKE operated by the Alfred-Wegener-institute. J. Large-Scale Res. Facilities 3, A210.

Baker, P., Mann, R., 2003. Late stage bivalve larvae in a well-mixed estuary are not inert particles. Estuaries 26 (4A), 837–845.

Baldwin, R.P., 1992. Cargo vessel ballast water as a vector for the spread of toxic phytoplankton species to New Zealand. J. R. Soc. N. Z. 22, 229–242.

Bartsch, J., Brander, K., Heath, M., et al., 1989. Modelling the advection of herring larvae in the North Sea. Nature 340, 632–636. https://doi.org/10.1038/340632a0.

Beermann, J., Gutow, L., Wührdemann, S., et al., 2023. Characterization and differentiation of sublittoral sandbanks in the southeastern North Sea. Biodivers. Conserv. 32, 2747–2768. https://doi.org/10.1007/s10531-023-02629-4.

Beng, K. C., Akimova, A., Androsov, A., Winter, C., Rahdarian, A., Sell, A. F., Pogoda, B., Stechele, B., Alter, K., Laakmann, S., Klemm, K., Sidorenko, V., Pineda-Metz, S. E. A., Rubinetti, S., Brand, S. C., & Schmittmann, L. (in preparation). Assessing connectivity between marine protected areas by integrating molecular methods and biophysical modelling: A case study for the European flat oyster (Ostrea edulis).

Bennema, F.P., Engelhard, G.H., Lindeboom, H., 2020. Ostrea edulis beds in the Central North Sea: delineation, ecology, and restoration. ICES J. Mar. Sci. 77 (7–8), 2694–2705. https://doi.org/10.1093/icesjms/fsaa134.

BfN: Bundesamt für Naturschutz, 2020a. Managementplan für das Naturschutzgebiet "Sylter Außenriff - Östliche Deutsche Bucht" (MPSyl). Bundesamt für Naturschutz, Bonn, Germany. https://www.bundesanzeiger.de/pub/publication/h0d1RV6aENhZ85BfVb3/content/200411001798M001/BAnzAT13052020B1100.pdf.

BfN: Bundesamt für Naturschutz, 2020b. Managementplan für das Naturschutzgebiet "Borkum Riffgrund" (MPBRg). Bundesamt für Naturschutz, Bonn, Germany. https://www.bfn.de/sites/default/files/2021-06/BAnzAT13052020B900%20%283%29.pdf.

Bigdeli, M., Mohammadian, A., Pilechi, A., Taheri, M., 2022. Lagrangian modeling of marine microplastics fate and transport: the state of the science. J. Marine Sc. Eng. 10 (4), 481. https://doi.org/10.3390/jmse10040481.

Bos, O.G., Duarte-Pedrosa, S., Didderen, K., Bergsma, J.H., Heye, S., Kamermans, P., 2023. Performance of European oysters (*Ostrea edulis* L.) in the Dutch North Sea, across five restoration pilots. Front. Mar. Sci. 10. https://doi.org/10.3389/fmars.2023.1233744.

Burchard, H., Hetland, R.D., 2010. Quantifying the contributions of tidal straining and gravitational circulation to residual circulation in periodically stratified tidal estuaries. J. Phys. Oceanogr. 40 (6), 1243–1262. https://doi.org/10.1175/2010jpo4270.1.

Callies, U., Groll, N., Horstmann, J., Kapitza, H., Klein, H., Maßmann, S., Schwichtenberg, F., 2017. Surface drifters in the German bight: model validation considering windage and stokes drift. Ocean Sci. 13 (5), 799–827. https://doi.org/10.5194/os-13-799-2017.

Carlton, J.T., 1985. Transoceanic and interoceanic dispersal of coastal marine organisms: the biology of ballast water. Oceanogr. Mar. Biol. Annu. Rev. 23, 313–371.

Carrasco, R., Horstmann, J., 2017. German bight surface drifter data from Heincke cruise HE 445, 2015. Panagaea. https://doi.org/10.1594/pangaea.874511.

Chegini, F., Holtermann, P., Kerimoglu, O., Becker, M., Kreus, M., Klingbeil, K., Gräwe, U., Winter, C., Burchard, H., 2020. Processes of stratification and Destratification during an Extreme River discharge event in the German bight ROFI. Journal of geophysical research. Oceans 125 (8). https://doi.org/10.1029/2019jc015987.

CMEMSa: Atlantic-European North West Shelf-Ocean Physics Analysis and Forecast, 2024. Copernicus Marine Service Information (CMEMS). Marine Data Store (MDS). Accessed on: 2024-06-24. https://doi.org/10.48670/moi-00054.

CMEMSb: Atlantic-European North West Shelf-Ocean Physics Reanalysis, 2024. Copernicus Marine Service Information. Marine Data Store (MDS). Accessed on: 2024-06-24. https://doi.org/10.48670/moi-00059.

Colsoul, B., Pouvreau, S., Di Poi, C., et al., 2020. Addressing critical limitations of oyster (*Ostrea edulis*) restoration: identification of nature-based substrates for hatchery production and recruitment in the field. Aquat. Conserv. Mar. Freshwat. Ecosyst. 30, 2101–2115. https://doi.org/10.1002/aqc.3454.

Colsoul, B., Boudry, P., Pérez-Parallé, M.L., Cetinic, A.N., Hugh-Jones, T., Arzul, I., Mérou, N., Wegner, K.M., Peter, C., Merk, V., Pogoda, B., 2021. Sustainable large-scale production of European flat oyster (Ostrea edulis) seed for ecological restoration and aquaculture: a review. Rev. Aquac. 13 (3), 1423–1468. https://doi.org/10.1111/raq.12529.

De Mesel, I., Kapasakali, D., Kerckhof, F., Vigin, L., Lacroix, G., Barbut, L., Degraer, S., 2018. *Ostrea edulis* Restoration in the Belgian Part of the North Sea: Feasibility Study. Royal Belgian Institute of Natural Sciences, Operational Directorate Natural Environment, Marine Ecology and Management, p. 89.

Dekshenieks, M.M., Hofmann, E.E., Klinck, J.M., Powell, E.N., 1996. Modeling the vertical distribution of oyster larvae in response to environmental conditions. Mar. Ecol. Prog. Ser. 136 (1–3), 97–110. https://doi.org/10.3354/meps136097.

Deyle, L., Badewien, T.H., Wurl, O., Meyerjürgens, J., 2023. Lagrangian surface drifter observations in the North Sea: an overview on high resolution tidal dynamics and submesoscale surface currents. Earth Syst. Sci. Data Discuss. 2023, 1–22.

Duran-Matute, M., Fajardo-Urbina, J.M., Giesbergen, M., Gräwe, U., Clercx, H.J.H., Gerkema, T., 2024. Lagrangian transport in a multiple-inlet coastal system: the difference between using 3D and depth-averaged currents. In: EGU General Assembly 2024, Vienna, Austria, 14–19 April 2024, EGU24-12817. https://doi.org/10.5194/egusphere-egu24-12817.

EEA, 2024. EEA Coastline for Analysis. https://www.eea.europa.eu/en/datahub/datahubitem-view/af40333f-9e94-4926-a4f0-0a787f1d2b8f. Accessed on: 2024-06-24.

Egbert, G.D., Erofeeva, S.Y., 2002. Efficient inverse modeling of Barotropic Ocean tides. J. Atmos. Ocean. Technol. 19 (2), 183–204. https://doi.org/10.1175/1520-0426(2002)019.

EMODnet, 2024. EMODnet Bathymetry Data. https://emodnet.ec.europa.eu/en/bathymetry; EMODnet Tide Gauge Data. https://emodnet.ec.europa.eu/en/physics#physics-products-sealevel. Accessed on: 2024-06-24.

ERA 5, 2024. ECMWF Reanalysis v5. https://www.ecmwf.int/en/forecasts/dataset/ecmwf-reanalysis-v5. Accessed on: 2024-06-24.

Ermgassen and others, 2023. Overcoming Ostrea edulis seed production limitations to meet ecosystem restoration demands in the UN decade on restoration. Aquat. Living Resour. 36, 16. https://doi.org/10.1051/alr/2023012.

EU blue economy report, 2023. Directorate-General for Maritime Affairs and Fisheries, Joint Research Centre. In: Borriello, A., Calvo Santos, A., Ghiani, M., et al. (Eds.), The EU blue economy report 2023. Publications Office of the European Union https://data.europa.eu/doi/10.2771/7151.

European Green Deal. https://commission.europa.eu/strategy-and-policy/priorities-2019-2024/story-von-der-leyen-commission/european-green-deal_en. https://ec.europa.eu/commission/presscorner/detail/en/fs_24_1391. Accessed on: 2024-06-24.

Fajardo-Urbina, J.M., Arts, G., Gräwe, U., Clercx, H.J.H., Gerkema, T., Duran-Matute, M., 2023. Atmospherically driven seasonal and interannual variability in the Lagrangian transport time scales of a multiple-inlet coastal system. J. Geophys. Res. Oceans 128, e2022JC019522. https://doi.org/10.1029/2022JC019522.

Fofonova, V., Others, 2021. Plume spreading test case for coastal ocean models. Geosci. Model Dev. 14 (11), 6945–6975. https://doi.org/10.5194/gmd-14-6945-2021.

Fofonova, V., Androsov, A., Sander, L., Kuznetsov, I., Amorim, F., Hass, C., Wiltshire, K. H., 2019. Non-linear aspects of the tidal dynamics in the Sylt-Rømø bight, South-Eastern North Sea. Ocean Sci. https://doi.org/10.5194/os-15-1761-2019.

Fox, A.D., Henry, L.A., Corne, D.W., Roberts, J.M., 2016. Sensitivity of marine protected area network connectivity to atmospheric variability. R. Soc. Open Sci. 3 (11), 160494.

Hahn, S.J., Brandt, A., Sonnewald, M., 2022. Annotated checklist and biodiversity analysis of benthic fauna at Sylt outer reef and Borkum reef ground (North Sea). Check List 18 (3), 593–628. https://doi.org/10.15560/18.3.593.

Hufnagl, M., Peck, M.A., Nash, R.D.M., Pohlmann, T., Rijnsdorp, A.D., 2012. Changes in potential North Sea spawning grounds of plaice (*Pleuronectes platessa* L.) based on early life stage connectivity to nursery habitats. Neth. J. Sea Res. 84. https://doi.org/10.1016/j.seares.2012.10.007.

Hughes, A., Others, 2023. Site selection for European native oyster (Ostrea edulis) habitat restoration projects: an expert-derived consensus. Aquat. Conserv. 33 (7), 721–736. https://doi.org/10.1002/aqc.3917.

Jain, A., Mao, N.J., Mohiuddin, K., 1996. Artificial neural networks: a tutorial. Computer 29 (3), 31–44. https://doi.org/10.1109/2.485891.

Kopte, R., Becker, M., Holtermann, P., Winter, C., 2022. Tides, stratification, and counter rotation: the German bight ROFI in comparison to other regions of freshwater influence. J. Geophys. Res. Oceans 127, e2021JC018236. https://doi.org/10.1029/2021JC018236.

Krause, J., Schuchardt, B., Boley-Fleet, K., Scheiffarth, G., Heinicke, K., Olischläger, J., Kruse, M., Südbeck, P., 2022. German marine protected areas in the North Sea - from the Wadden Sea to the exclusive economic zone. Natur und Landschaft. https://doi.org/10.19217/NuL2022-01-01.

Kuznetsov, I., Androsov, A., Fofonova, V., Danilov, S., Rakowsky, N., Harig, S., Wiltshire, K.H., 2020. Evaluation and application of newly designed finite volume coastal model FESOM-C, effect of variable resolution in the southeastern North Sea. Water 12, 1412. https://doi.org/10.3390/w12051412.

Lapègue, S., Reisser, C., Harrang, E., Heurtebise, S., Bierne, N., 2023. Genetic parallelism between European flat oyster populations at the edge of their natural range. Evol. Appl. 16, 393–407. https://doi.org/10.1111/eva.13449.

Maathuis, M.A.M., Coolen, J.W.P., van der Have, T., Kamermans, P., 2020. Factors determining the timing of swarming of European flat oyster (Ostrea edulis L.) larvae

in the Dutch Delta area: implications for flat oyster restoration. J. Sea Res. 156, 101828. https://doi.org/10.1016/j.seares.2019.101828.
MarGate Underwater Observatory. https://www.awi.de/en/science/special-groups/scientific-diving/margate.html, 2024. Accessed on: 2024-06-24.
Mayorga-Adame, C.G., Polton, J.A., Fox, A.D., Henry, L.A., 2022. Spatiotemporal scales of larval dispersal and connectivity among oil and gas structures in the North Sea. Mar. Ecol. Prog. Ser. 685, 49–67.
Meyerjürgens, J., Others, 2023. Sources, pathways, and abatement strategies of macroplastic pollution: an interdisciplinary approach for the southern North Sea. Front. Mar. Sci. 10, 1148714. https://doi.org/10.3389/fmars.2023.1148714.
Meyerjürgens, J., Badewien, T.H., Garaba, S.P., Wolff, J.O., Zielinski, O., 2019. A state-of-the-art compact surface drifter reveals pathways of floating marine litter in the German bight. Front. Mar. Sci. 6, 58. https://doi.org/10.3389/fmars.2019.00058.
Meyerjürgens, J., Deyle, L., Meyer-Hagg, L., Janssen, E., Butter, M., Braun, A., Zielinski, O., Badewien, T.H., 2023. Surface drifter North Sea 2017-2021. PANGAEA. https://doi.org/10.1594/PANGAEA.963166.
Möhler, J., Wegner, M., Reise, K., Jacobsen, S., 2011. Invasion genetics of Pacific oyster Crassostrea gigas shaped by aquaculture stocking practices. J. Sea Res. 66, 256–262. https://doi.org/10.1016/j.seares.2011.08.004.
Molen, J.V.D., García-García, L.M., Whomersley, P., et al., 2018. Connectivity of larval stages of sedentary marine communities between hard substrates and offshore structures in the North Sea. Sci. Rep. 8, 14772. https://doi.org/10.1038/s41598-018-32912-2.
Neder, C., Fofonova, V., Androsov, A., Kuznetsov, I., Abele, D., Falk, U., Jerosch, K., 2022. Modelling suspended particulate matter dynamics at an Antarctic fjord impacted by glacier melt. J. Mar. Syst. 103734. https://doi.org/10.1016/j.jmarsys.2022.103734.
OSPAR, 2020. Status Assessment 2020 - European flat oyster and *Ostrea edulis* beds. https://oap.ospar.org/en/ospar-assessments/committee-assessments/biodiversity-committee/status-assesments/european-flat-oyster/. Accessed on: 2024-06-24.
Pastor Rollan, A., Ospina-Álvarez, A., Larsen, J., Thorbjørn Hansen, F., Schourup-Kristensen, V., Maar, M., 2023. A sensitivity analysis of mussel larvae dispersal in a Danish estuary based on a biophysical model. Reg. Stud. Mar. Sci. 68, 103260. https://doi.org/10.1016/j.rsma.2023.103260.
Pineda-Metz, S. E. A., Schittmann, L., Sidorenko, V., Androsov, A., Rubinetti, S., & Pogoda, B. (in preparation). Should I stay or should I go: Larval dispersal models as a support tool for oyster restoration.
Pogoda, B., Others, 2020. NORA moving forward: developing an oyster restoration network in Europe to support the Berlin oyster recommendation. Aquat. Conserv. 30 (11), 2031–2037. https://doi.org/10.1002/aqc.3447.
Pogoda, B., Others, 2023. Come, Tell me how you Live: Habitat Suitability Analysis for *Ostrea edulis* Restoration. Marine and Freshwater Ecosystems. Portico, Aquatic Conservation. https://doi.org/10.1002/aqc.3928.
Pogoda, B., Brown, J., Hancock, B., Preston, J., Pouvreau, S., Kamermans, P., Sanderson, W., Von Nordheim, H., 2019. The native oyster restoration Alliance (NORA) and the Berlin oyster recommendation: bringing back a key ecosystem engineer by developing and supporting best practice in Europe. Aquat. Living Resour. 32, 13. https://doi.org/10.1051/alr/2019012.
Reise, K., Buschbaum, C., Büttger, H., Wegner, K.M., 2017. Invading oysters and native mussels: from hostile takeover to compatible bedfellows. Ecosphere 8 (9), e01949. https://doi.org/10.1002/ecs2.19497.
Ricker, M., Meyerjürgens, J., Badewien, T.H., Stanev, E.V., 2022. Lagrangian methods for visualizing and assessing frontal dynamics of floating marine litter with a focus on tidal basins. In: The handbook of environmental chemistry book series (HEC, volume 116). https://doi.org/10.1007/978-3-662-65839-0_1017.
Robert, R., His, E., Dinet, A., 1988. Combined effects of temperature and salinity on fed and starved larvae of the European flat oyster Ostrea edulis. Mar. Biol. 97, 95–100.
Robert, R., Vignier, J., Petton, B., 2017. Influence of feeding regime and temperature on development and settlement of oyster Ostrea edulis (Linnaeus, 1758) larvae. Aquac. Res. https://doi.org/10.1111/are.13297.
Rodriguez-Perez, A., Sanderson, W.G., Møller, L.F., Henry, T.B., James, M., 2020. Return to sender: the influence of larval behaviour on the distribution and settlement of the European oyster *Ostrea edulis*. Aquatic Conserv: Mar Freshw Ecosyst. 30, 2116–2132. https://doi.org/10.1002/aqc.3429.
Rubinetti, S., Fofonova, V., Arnone, E., Wiltshire, K.H., 2023. A complete 60-year catalog of wind events in the German bight (North Sea) derived from ERA5 reanalysis data. Earth and Space Sci. 10 (10), e2023EA003020. https://doi.org/10.1029/2023EA003020.
Schourup-Kristensen, V., Larsen, J., Stæhr, P.A.U., Maar, M., 2023. Modelled dispersal pathways of non-indigenous species in the Danish Wadden Sea. Mar. Environ. Res. 191, 106111.
Schrum, C., 1997. Thermohaline stratification and instabilities at tidal mixing fronts: results of an eddy resolving model for the German bight. Cont. Shelf Res. 17 (6), 689–716. https://doi.org/10.1016/s0278-4343(96)00051-9.
Sidhu, C., Others, 2023. Dissolved storage glycans shaped the community composition of abundant bacterioplankton clades during a North Sea spring phytoplankton bloom. Microbiome 11 (1). https://doi.org/10.1186/s40168-023-01517-x.
SMS, 2024. Automated process for mesh generation, SMS 13.3. https://s3.amazonaws.com/smstutorials-13.3.aquaveo.com/SMS_MeshGeneration.pdf. Accessed on: 2024-06-24.
Sprong, P., Fofonova, V., Wiltshire, K.H., Neuhaus, S., Ludwichowski, K.-U., Käse, L., Androsov, A., Metfies, K., 2020. Spatial dynamics of eukaryotic microbial communities in the German bight. J. Sea Res. https://doi.org/10.1016/j.seares.2020.101914.
Stanev, E.V., Others, 2019. Extreme westward surface drift in the North Sea: public reports of stranded drifters and Lagrangian tracking. Cont. Shelf Res. 177, 24–32. https://doi.org/10.1016/j.csr.2019.03.003.
Stanev, E.V., Jacob, B., Pein, J., 2019. German bight estuaries: an inter-comparison on the basis of numerical modeling. Cont. Shelf Res. 174, 48–65. https://doi.org/10.1016/j.csr.2019.01.001.
Stechele, B., et al., 2023. Northern Europe's suitability for offshore European flat oyster (*Ostrea edulis*) habitat restoration based on population dynamics. Front. Mar. Sci. 10. https://doi.org/10.3389/fmars.2023.1224346.
Ter Hofstede, R., Witte, S., Kamermans, P., van Koningsveld, M., Tonk, L., 2024. Settlement success of European flat oyster (*Ostrea edulis*) on different types of hard substrate to support reef development in offshore wind farms. Ecol. Eng. 200, 107189. https://doi.org/10.1016/j.ecoleng.2024.107189.
TPXO 9, 2024. TPXO9-atlas. https://www.tpxo.net/global/tpxo9-atlas. Accessed on: 2024-06-24.
Visser, A.W., 1994. On tidal rectification, friction, and geostrophic degeneracy. J. Phys. Oceanogr. 24 (10), 2196–2200. https://doi.org/10.1175/1520-0485(1994)024.
Vogel, C., Ripken, M., Klenke, T., 2018. Linking marine ecosystem services to the North Sea's energy fields in transnational marine spatial planning. Environments 5 (6), 67. https://doi.org/10.3390/environments5060067.
Wang, Y., Raitsos, D.E., Krokos, G., Zhan, P., Hoteit, I., 2022. A Lagrangian model-based physical connectivity atlas of the Red Sea coral reefs. Front. Mar. Sci. 9, 925491. https://doi.org/10.3389/fmars.2022.925491.
Wiltshire, K.H., 2017. Urbanization of coastal and shelf seas. In: Conference Proceedings COME 2017 Decommissioning of Offshore Geotechnical, COME - Decommissioning 2017. TUHH Hamburg University of Technology hdl:10013/epic.51728.